



## Cytotoxicity and DNA binding of Manganese (II) complex Containing pyridine ligand

Alaa A. Al-Yaseen<sup>1</sup>, Mouayed A. Hussein<sup>2</sup>

<sup>1,2</sup> University of Basrah, College of Science, Department of Chemistry, Basrah, Iraq.

Author Email: pgs.alaa.ayad@uobasrah.edu.iq

### Abstract

Received: 25.12.2024

Revised: 01.05.2025

Accepted: 15.05.2025

DOI:

10.32792/jmed.2025.29.5

#### Keywords:

Mn (II)

2-acetyl-6-bromopyridine  
oxime

DNA interaction  
cytotoxicity  
anticancer

The interaction between large biomolecules and ligands has attracted considerable interest due to its biological properties. Calf thymus DNA (CT-DNA) can interact with biologically active compounds to form complexes. DNA is a primary target for anticancer drugs that are involved in important cellular processes. The ligand and the manganese complex  $\text{MnCl}_2 \cdot (2\text{-acetyl-6-bromopyridine oxime})_2$  were synthesized. The ligand was examined using infrared spectroscopy, CHN,  $^1\text{H}$ NMR, and  $^{13}\text{C}$ NM techniques. CHN elemental analysis and infrared spectroscopy were also used to analyze the complex. Both compound 1 and the ligand demonstrated cross-linking with calf thymus DNA (CT-DNA), and the complex demonstrated higher binding efficiency than the ligand alone. The in vitro toxicity of compound 1 was evaluated using metabolic assays using 3-(4,5-dimethylthiazol-2-yl)-2,5-diphenyltetrazolium bromide as an anticancer agent against esophageal cancer cells (SKGT-4). In SKGT-4 cells, the compound showed a significant inhibitory effect. Therefore, it could be proposed as a future anticancer drug due to its low cytotoxicity.

Alaa A. Al-Yaseen, Mouayed A. Hussein 2.  
Cytotoxicity and DNA binding of  
Manganese (II) complex Containing  
pyridine ligand. Thi-Qar Medical Journal  
(TQMJ). 2025;29(3006-4791):1-10.

Copyright: ©2025 The authors. This article is published by the Thi-Qar Medical Journal and is licensed under the CC BY 4.0 license

### 1. Introduction

The most common forms,  $\text{Mn}^{2+}$  and  $\text{Mn}^{3+}$ , are found in living tissues and can be used as MRI contrast materials because of their paramagnetic properties. Manganese, an important transition metal with the atomic number 25 and the electronic configuration  $[\text{Ar}]3d^54s^2$  has an oxidation state ranging from -3 to +7 [1]. Manganese coordination compounds are effective anticancer drugs because of their physical and chemical characteristics, which are remarkably similar to those of iron and make manganese a necessary micronutrient for most environmental organisms. The second reason is that manganese (Mn) is an essential cofactor for many dominant enzymes (biological catalysts), more so than any other mineral. Third, the fact that it is the second most prevalent transition metal on Earth proves its availability. Fourth, with oxidation states ranging from -3 to +7, the most common in nature, the most studied, and the safest for human health are +2, +3, and +4 [2]. Luminous metal-to-ligand charge transfer (MLCT) excited states, commonly

observed in precious metal complexes with the d6 valence electron configuration, are the basis for several applications in lighting, sensing, solar cells, and synthetic photochemistry [3]. Mn<sup>2+</sup> ions are present in manganese ferrite, an inorganic substance that is frequently employed in adsorption, desorption, and magnetic drug targeting/delivery procedures. Manganese ferrite is a heat-resistant, non-corrosive, environmentally benign, non-toxic, high-impact resistant, reusable material [4]

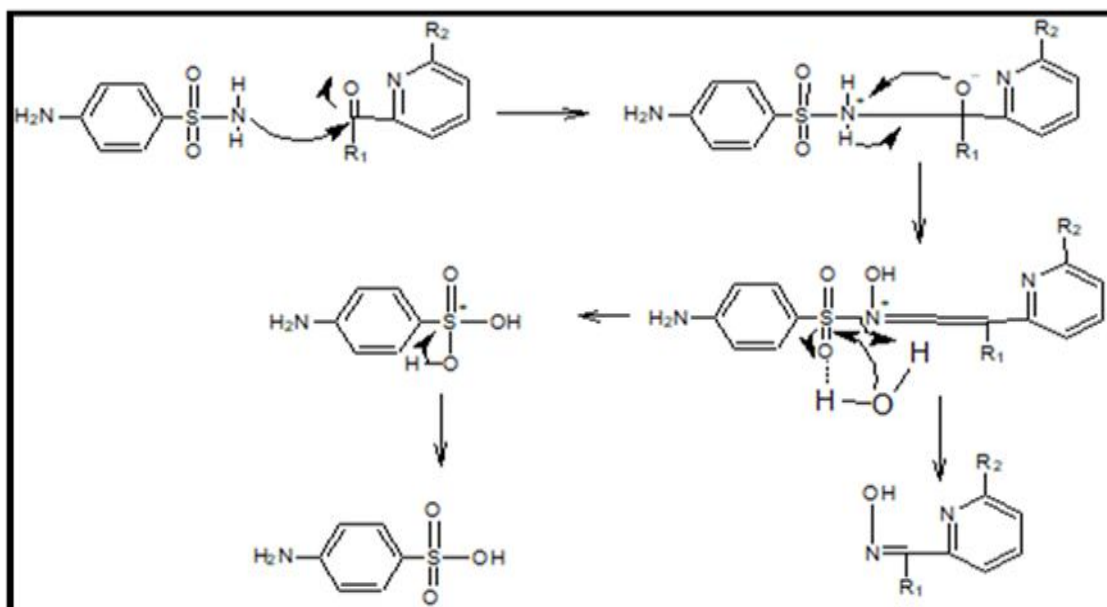
### 1.1. Methodology and Approaches

The materials were obtained from Aldrich and Hangzhou Hyper Company and the toxicity of the prepared ligand and complex and their ability to bind to CT-DNA were evaluated using a Gallen-Kamp MFB-600 device. The melting point was measured and the proton and carbon 13 NMR spectra of the resulting ligand in this work were obtained using a 400 MHz ascending device in the Chemistry Department, College of Education for Pure Sciences, University of Basrah using the solvent (Dimethylsulfoxide-d<sub>6</sub>) from BRUKER Company, and in the Chemistry Department, College of Science, University of Basrah, the FTIR of the resulting ligand and complex was measured using ALPHA II device from BRUKER Company, Germany.

## 2. Synthesis

### 2.1. 2-acetyl-6-bromopyridine oxime synthesis

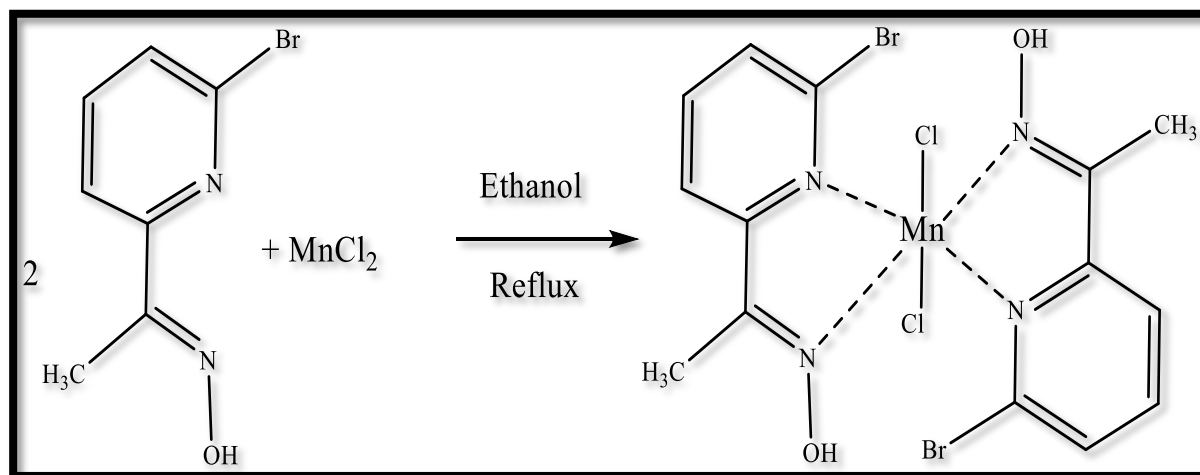
A 15 ml methanolic solution of 2-acetyl-6-bromopyridine (0.825 g, 4.127 mmol) was added to a solution of p-aminobenzene sulfonamide (0.710 g, 4.127 mmol) in methanol. For two hours, the mixture was refluxed while being stirred. When chilled and cured for a few days at room temperature, translucent crystals were produced with a Yield of 67 %. The molar mass of the final product was 215 g/mol. The spectra revealed the IR basic vibration modes: ( $\nu$  cm.<sup>-1</sup>), C=N (1639w), CH (1477s), N-O (996m), and -O-H (2916s). The analysis for C<sub>7</sub>H<sub>7</sub>BrN<sub>2</sub>O was computed as follows: C, 39.10; H, 3.28; N, 13.03; discovered as C, 39.13; H, 3.32; N, 13.1). 1.16 (s, 3H, CH<sub>3</sub>), 8.15 (m, 1H, Ar-H), 8.58 (m, 1H, Ar-H), 9.18 (m, 1H, Ar-H), and 10.09 (s, 1H, OH) are the <sup>1</sup>H-NMR  $\delta$  ppm (400 MHz, DMSOd<sub>6</sub>). <sup>13</sup>CNMR:  $\delta$  ppm (400 MHz, DMSOd<sub>6</sub>), aromatic carbons at 124.14-148.14, 11.47 for CH<sub>3</sub>, C=N group 153.14. This ligand was prepared according to the method described in Scheme 1 [5].



Scheme 1. Synthesis route of ligands

## 2.2. [Di chloro di {2-acetyl-6-bromopyridine oxime} manganese(II)] MnL Synthesis

Scheme 2 shows the pathway for the preparation of the MnL complex. Drop by drop, a methanolic solution of L2 (0.837 g, 4.124 mmol) was mixed with a methanolic  $\text{MnCl}_2 \cdot 2\text{H}_2\text{O}$  (0.408 g, 2.0635 mmol). For three hours, the reaction mixture was left to reflux. After filtering, the resulting solution was stored at room temperature. After being cooled and let sit at room temperature for a few days, transparent crystals were produced with a yield of 68 %. The resulting prepared compound had a molar mass of 555.9 g/mol. The analysis for  $\text{C}_{14}\text{H}_{14}\text{Br}_2\text{Cl}_2\text{MnN}_4\text{O}_2$  was calculated: C, 30.25; H, 2.54; N, 10.08; Found: C, 31.30; H, 2.89; N, 10.96; The spectra showed the IR fundamental vibration modes: ( $\nu$   $\text{cm}^{-1}$ ), (C=N) at 1631, and (N=C-CH<sub>3</sub>) that emerged at 998 and 1477.



Scheme 2. General synthetic route of complexes MnL.

Table 1: Physical properties of the prepared compounds (ligand and complex)

Comp.	Compounds Structure	Chemical formula	Atomic Weight	Color of crystals	Melting Point °C	Yield %
L		$\text{C}_7\text{H}_7\text{BrN}_2\text{O}$	215	Transparent	172-180	67
MnL		$\text{C}_{14}\text{H}_{14}\text{Br}_2\text{Cl}_2\text{MnN}_4\text{O}_2$	555.9	transparent crystals	Disintegration 182-190	68

### **3. Cytotoxicity studies**

#### **3.1. Cell culture preparation**

Esophageal cancer (SK-GT-4) cells were implanted under optimal incubation conditions. Cell plating was chosen from cells that had a consistency level of 70–80%, and aspiration was used in place of the previous medium. Sterile phosphate-buffered saline (pH 7.4) was then used to clean the cells two or three times. Then, the intact layer of the connected cells was trypsinized. Following three to five minutes of incubation in 5% CO<sub>2</sub> at 37 °C, the flasks holding the cells were lightly tapped to promote cell segregation. Using an inverted microscope, the complete cell segregation was detected. The addition of five milliliters of recently finished medium containing 10% fetal bovine serum decreased the activity of trypsin. Following cell dilution and counting.

#### **3.2. MTT assay**

The highest significant IC<sub>50</sub> values for SK-GT-4 esophageal cancer cell lines were determined using the MTT test. MTT is used as an endpoint assay to assess cell viability at a specific time. The experiments were conducted on a lung cancer cell line. The cytotoxicity was expressed as the IC<sub>50</sub>, which is the concentration that reduces treated cell absorbance by 50%. The 560 nm absorbance was then measured using an ELISA plate reader. The data was evaluated to estimate the effect of the complexes on cell viability, where cell viability (%) = [OD (sample) / OD (control)] × 100, and then the growth inhibition percentage was computed [6].

### **4. DNA binding experiments**

#### **4.1. Absorption spectral studies**

Spectroscopic and physical techniques assessed the ligands' and their Mn(II) complexes' binding to calf thymus DNA (CT-DNA). The binding with DNA was monitored spectrophotometrically using fixed concentrations of the ligands or complexes (10 µM) with increasing amounts of DNA (10-100 µM) in a 6.3 mM Tris-HCl/50 mM NaCl buffer (pH=7.2). Alternatively, the physical binding with DNA at 37 °C was followed using a fixed concentration of DNA (10 µM) with increasing levels of the ligand or complexes, where the ratio of concentration (r): 1-10, where  $r = [\text{complex}] / [\text{DNA}]$ .

#### **4.2. Viscosity measurements.**

Without crystallographic structural information, hydrodynamic techniques sensitive to length change-such as viscosity and sedimentation-are thought to be among the most precise and unambiguous evaluations of a binding mode in solution. The variations in DNA length brought about by its various binding mechanisms with guest molecules significantly affect the sensitivity of viscosity measurement. It is anticipated that ligand intercalating agents, such as conventional intercalations, will lengthen the double helix to insert tiny molecules between the bases, increasing the viscosity of DNA [7]. Conversely, a partial and/or non-classical ligand intercalation may cause the DNA helix to bend or kink, decreasing its effective length and viscosity simultaneously.  $(\eta/\eta_0)^{1/3}$  values were plotted against  $[\text{complex}]/[\text{DNA}]$ , where  $\eta$  and  $\eta_0$  represent the relative viscosities of DNA with and without MnL. According to the plot of Fig. 1, exhibits comparatively minor alterations in DNA viscosity, suggesting that they bind to DNA weakly, which is in line with the previously proposed DNA groove binding [9].

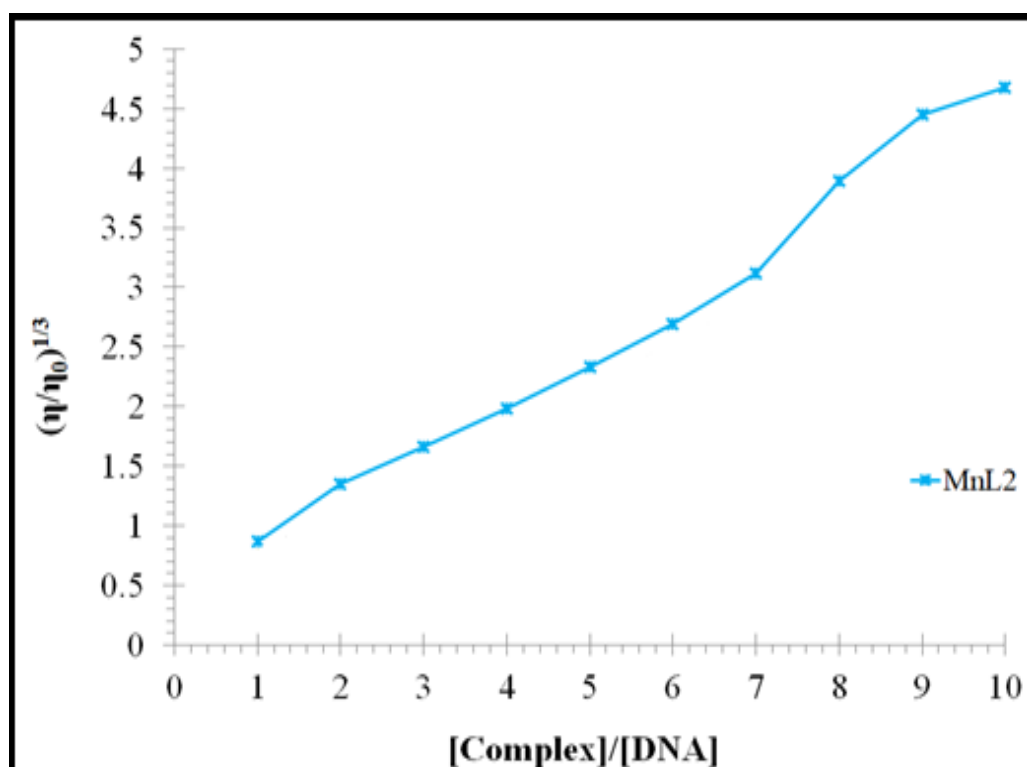
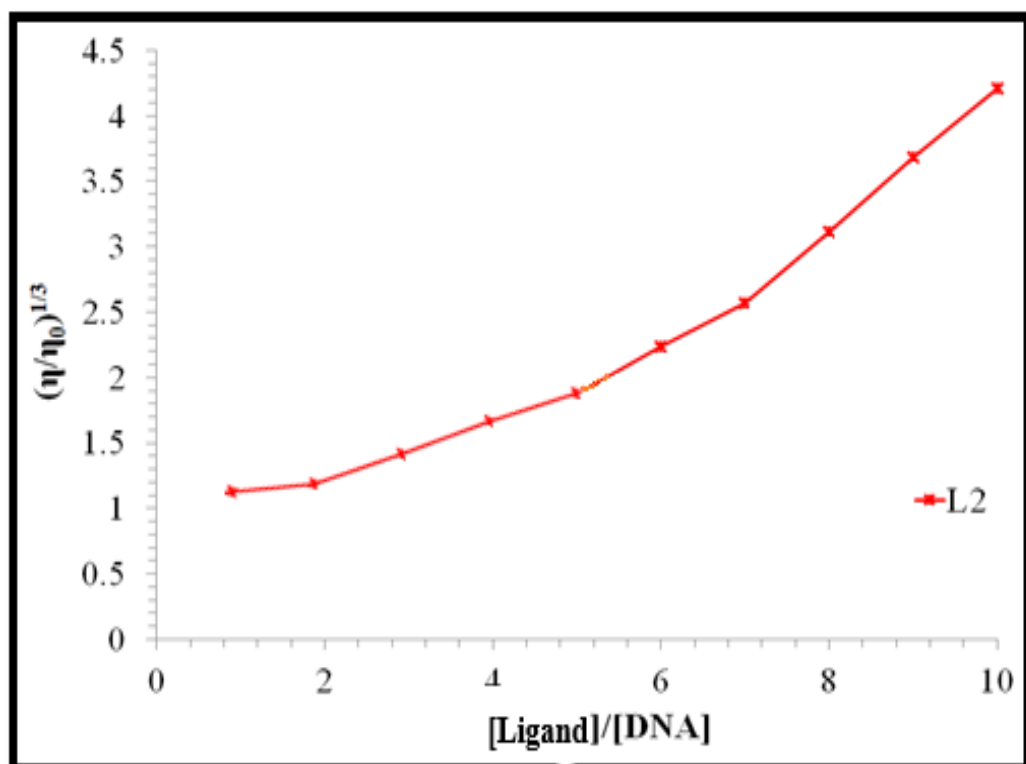


Fig. 1. Effect of increasing amounts of the ligand and complex on the relative viscosities of CT DNA in 6.3 mM Tris-HCl/50 mM NaCl buffer (pH= 7.2).

## 5. Results

### 5.1. Absorption spectroscopy

UV-Vis spectroscopy is one of the most popular techniques for describing how metal complexes bind to DNA. Generally speaking, the complexes can attach to DNA by covalent means such as substituting the guanine N7 of DNA for an unstable ligand of the complex, or by non-covalent means like interference, electrostatic contact, or groove binding [8]. When DNA is present, the molecules' absorption intensity may rise (hyperchromia) or fall (hypochromia). The ligand and complex 1 absorption spectra are displayed in Figure 2. As demonstrated, a notable hypochromic impact was produced by the slow addition of CT-DNA, signifying the interference interaction with CT-DNA.

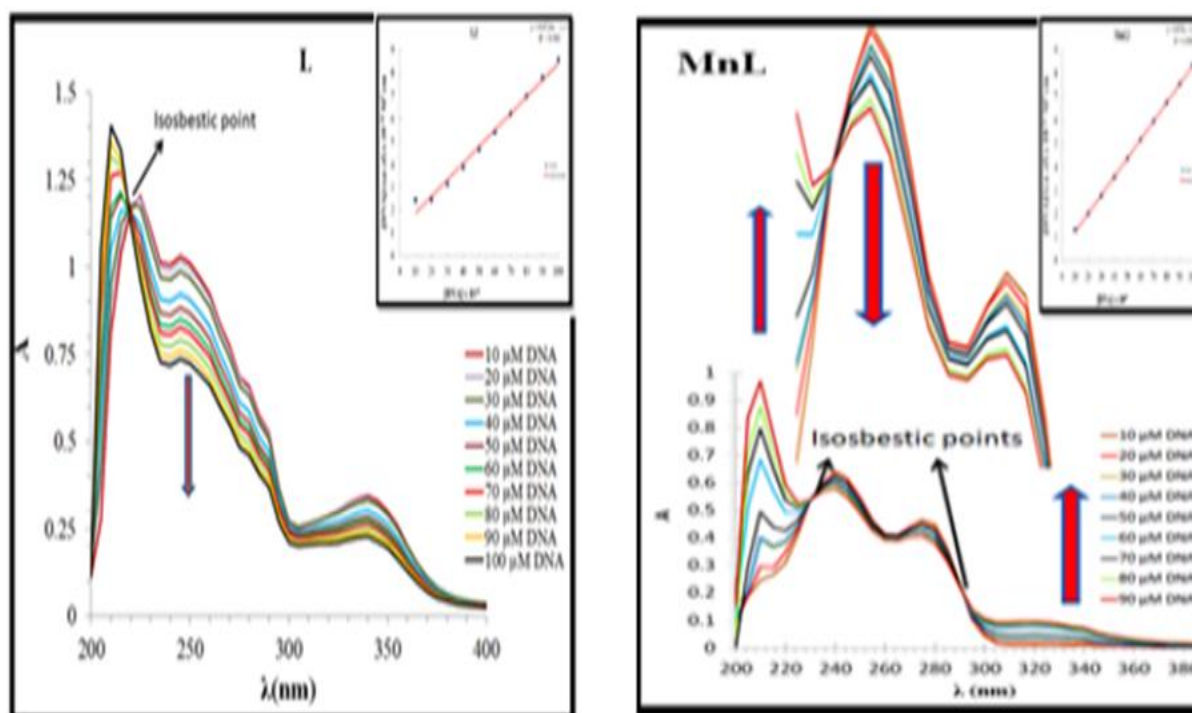


Fig. 2. The electronic absorption spectrum of L and MnL in 6.3 mM Tris-HCl/50 mM NaCl buffer (pH= 7.2) in the presence of CT DNA at increasing amounts. The arrow shows the changes in absorbance upon increasing amounts of CT DNA

The intrinsic binding constant  $K_b$  was estimated using the following equation [10] based on the change in absorbance with an increase in the amount of CT DNA. The formula is:

$$\frac{[DNA]}{\epsilon_a - \epsilon_f} = \frac{[DNA]}{\epsilon_b - \epsilon_f} + \frac{1}{k_b}(\epsilon_b - \epsilon_f) \quad \dots\dots\dots (1)$$

$\text{Abs}/[DNA]$ , the extinction coefficient for the free complex, and the extinction coefficient for the complex in the fully bound form are represented by the absorption coefficients  $\epsilon_a$ ,  $\epsilon_f$ , and  $\epsilon_b$ , respectively. (Figure 2) illustrates a plot of  $[DNA]/(\epsilon_b - \epsilon_f)$  vs  $[DNA]$ , which yielded a slope of  $1/(\epsilon_b - \epsilon_f)$  and an intercept of  $1/k_b$  ( $\epsilon_b - \epsilon_f$ ). The 260 nm and 270 nm electron transitions were selected to track the ligand and complex spectral hypochromism behavior.

### 5.2. Viscosity measurements

To further validate the interaction with CT DNA, viscometric investigations were also conducted. Base pairs are pushed apart when a chemical intercalates into DNA, extending the helix and making it more viscous.



But because the medication's molecule might Bending the DNA helix reduces its effective length and, as a result, its viscosity. The DNA structure is destroyed by electrostatic or groove binding. The purpose of the viscosity measurements was to shed further light on how complex 1 and the ligand interact with DNA. As the concentration of the ligand and complex increases, the relative viscosity  $(\eta/\eta_0)^{1/3}$  plotted against [DNA] (Fig. 2) demonstrates a notable rise in DNA relative viscosity [11]. The intercalative binding mechanism with DNA is shown by these results.

### 5.3. Antitumor activity of the complexes

Following the complex's first measurements, the MTT assay was used to assess the compound's detrimental impact on the human esophageal cancer cell line SK-GT-4, and the cytotoxic effect was investigated 72 hours later. At dosages ranging from 3 to 100  $\mu\text{g/ml}$ , the compound's detrimental effects on SK-GT-4 cells led to a dose-dependent decline in cell viability. Figure 4 demonstrates that SK-GT-4 cells had the lowest viability rate (89%), at a dose of 100  $\mu\text{g/ml}$ . With an  $\text{IC}_{50}$  of 18.06  $\mu\text{M}$ , the results also demonstrated a considerable suppression of cell growth in the cell lines. As seen in Figure 8, there was a strong correlation

between the compound's increased concentration and its inhibitory activity on cell proliferation. When compared to the untreated cells (control group), the SKGT-4 cell lines treated with the chemical displayed.

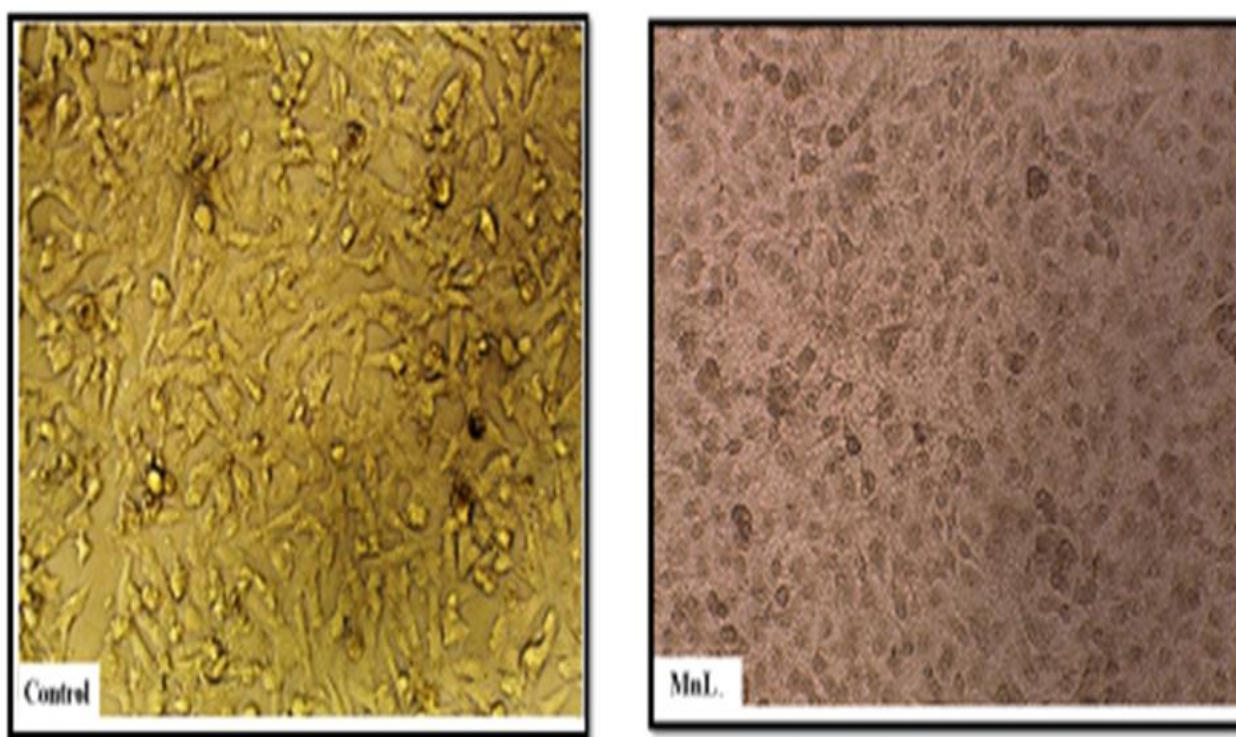
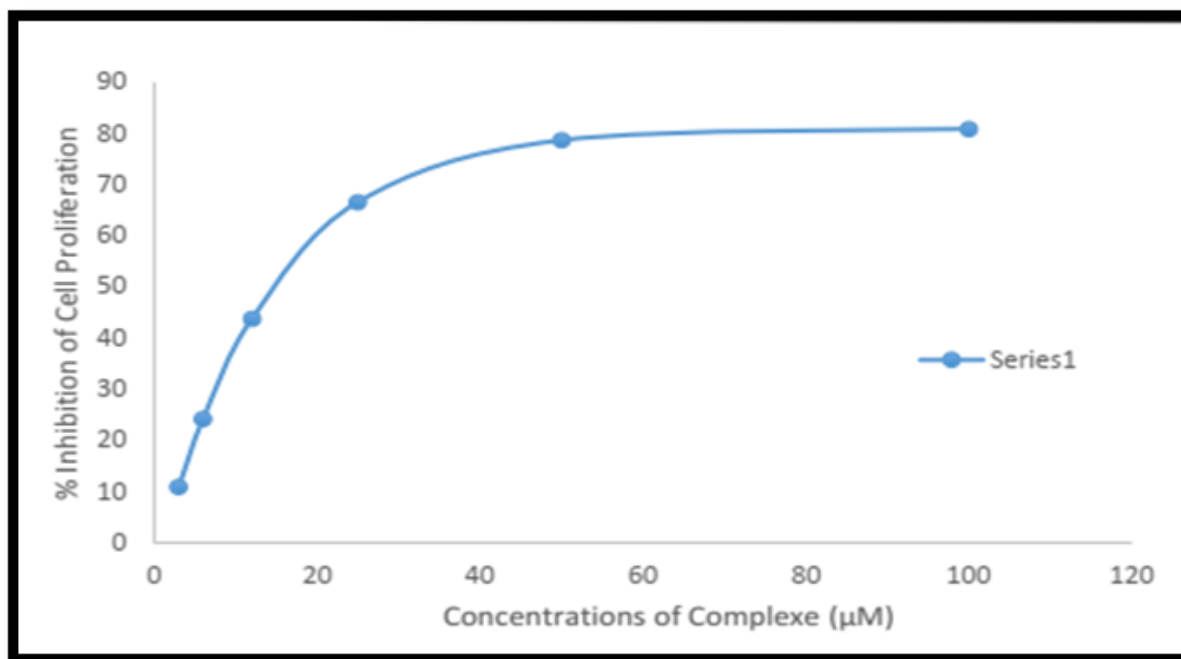


Fig. 3. Control untreated SK-GT-4 cells and Morphological changes on SK-GT-4 cell line after being treated with complexes MnL2



**Fig. 4. Inhibition of cell proliferation by the Mn(II) complexes**

## 6. Conclusion

A Mn (II) compound with 2-acetyl-6-bromo pyridine oxime was made for this investigation. The complex's antitumor activity was assessed in vitro after it was produced and structurally described. The Mn(II) complex exhibited the greatest value, and the results verified that both the ligand and the complex bind to CT-DNA. The compound was found to be a strong anti-metastatic agent against SK-GT-4 cell lines, which are human esophageal cancer. The complex's cytotoxic action is supported by the hydrogen bonding network in the molecular structure [12]. The complex may be regarded as a component of the research and development process for successful anticancer medicines, according to the study's findings.

## Acknowledgments

I want to thank everyone who helped make this study at the University of Basra a success, especially my supervisor, prof. Dr. Mouayed A. Hussein, for his advice and encouragement.

## REFERENCES

1. Sguizzato, M., et al., Manganese in diagnostics: a preformulatory study. *Pharmaceutics*, 2022. 14(1): p. 108. <https://doi.org/10.3390/pharmaceutics14010108>
2. Odularu, A.T., MThe intrinsic binding constant  $K_b$  was estimated using the following equation [9] based on the change in absorbance with an increase in the amount of CT DNA. The formula is:  $\log K_b = \log K_{app} - \log(1 + \frac{[DNA]}{K_{app}})$ . The formula is:  $\log K_b = \log K_{app} - \log(1 + \frac{[DNA]}{K_{app}})$ . *Journal of Chemistry*, 2022. 2022. <https://doi.org/10.1155/2022/7062912>
3. Heinze, K., Made with manganese. *Nature Chemistry*, 2021. 13(10): p. 926-928. <https://doi.org/10.1038/s41557-021-00785-0>
4. Dippong, T., E.A. Levei, and O. Cadar, Recent advances in synthesis and applications of mfe2o4 (m= co, cu, mn, ni, zn) nanoparticles. *Nanomaterials*, 2021. 11(6): p. 1560.
5. Al-Yaseen, A.A. and M.A. Hussein, The first type of binuclear copper complex with terminal sulfide: synthesis, structural characterization, and cytotoxicity evaluation. *Journal of Sulfur Chemistry*, 2024: p. 1. <https://doi.org/10.1080/17415993.2024.2416237>



6. Wei, Z., S. Abbaspour, and R. Tayebbe, Nickel nanoparticles originated from cressa leaf extract in the preparation of a novel Melem@ Ni-HPA photocatalyst for the synthesis of some chromenes and a preliminary MTT assay on the anticancer activity of the nanocomposite. *Polycyclic Aromatic Compounds*, 2023. 43(1): p. 552-571. <https://doi.org/10.1080/10406638.2021.2019063>
7. Goudarziafshar, H., et al., Template synthesis, DNA binding, antimicrobial activity, Hirshfeld surface analysis, and 1D helical supramolecular structure of a novel binuclear copper (II) Schiff base complex. *RSC advances*, 2022. 12(22): p. 13580-13592. <https://doi: 10.1039/d2ra00719c>
8. Aderinto, S.O., et al., Iridium (III)-based minor groove binding complexes as DNA photocleavage agents. *Dalton Transactions*, 2024. 53(17): p. 7282-7291. <https://doi.org/ 10.1039/d4dt00171k>
9. Hussein, M.A. and A.A. Yaseen, New binuclear Cu (II) complex: synthesis, structural elucidation, cytotoxic and DNA-binding evaluation. *Transition Metal Chemistry*, 2024. 49(1): p. 53-62. <https://doi.org/10.1007/s11243-023-00561-8>
10. Abdel-Rahman, L.H., et al., Novel Bromo and methoxy substituted Schiff base complexes of Mn (II), Fe (III), and Cr (III) for anticancer, antimicrobial, docking, and ADMET studies. *Scientific reports*, 2023. 13(1): p. 3199. <https://doi.org/10.1038/s41598-023-29386-2>.
11. Shahabadi, N., S. Fatahi, and M. Maghsudi, Synthesis of a new Pt (II) complex containing valganciclovir drug and calf-thymus DNA interaction study using multispectroscopic methods. *Journal of Coordination Chemistry*, 2018. 71(2): (p. 258-270. <https://doi.org/10.1080/00958972.2018.1433828>
12. Ali, A., et al., Ligand substituent effect on the cytotoxicity activity of two new copper (ii) complexes bearing 8-hydroxyquinoline derivatives: Validated by MTT assay and apoptosis in MCF-7 cancer cell line (human breast cancer). *RSC advances*, 2021. 11(24): p. 14362-14373. <https://dio: 10.1039/D1RA00172H>